J. Fluid Mech. (2002), *vol.* 462, *pp.* 111–132.
DOI: 10.1017/S0022112002008492 Printed in the United Kingdom

The effect of viscous heating on the stability of Taylor–Couette flow

By U. A. AL-MUBAIYEDH†, R. SURESHKUMAR AND B. KHOMAMI

Department of Chemical Engineering and Materials Research Laboratory, Washington University, St. Louis, MO 63130, USA

(Received 18 December 2000 and in revised form 25 January 2002)

The influence of viscous heating on the stability of Taylor–Couette flow is investigated theoretically. Based on a linear stability analysis it is shown that viscous heating leads to significant destabilization of the Taylor–Couette flow. Specifically, it is shown that in the presence of viscous dissipation the most dangerous disturbances are axisymmetric and that the temporal characteristic of the secondary flow is very sensitive to the thermal boundary conditions. If the temperature difference between the two cylinders is small, the secondary flow is stationary as in the case of isothermal Taylor–Couette flow. However, when the temperature difference between the two cylinders is large, time-dependent secondary states are predicted. These linear stability predictions are in agreement with the experimental observations of White & Muller (2000) in terms of onset conditions as well as the spatiotemporal characteristics of the secondary flow. Nonlinear stability analysis has revealed that over a broad range of operating conditions, the bifurcation to the time-dependent secondary state is subcritical, while stationary states result as a consequence of supercritical bifurcation. Moreover, the supercritically bifurcated stationary state undergoes a secondary bifurcation to a time-dependent flow. Overall, the structure of the time-dependent state predicted by the analysis compares very well with the experimental observations of White & Muller (2000) that correspond to slowly moving vortices parallel to the cylinder axis. The significant destabilization observed in the presence of viscous heating arises as the result of the coupling of the perturbation velocity and the base-state temperature gradient that gives rise to fluctuations in the radial temperature distribution. Due to the thermal sensitivity of the fluid these fluctuations greatly modify the fluid viscosity and reduce the dissipation of disturbances provided by the viscous stress terms in the momentum equation.

1. Introduction

It is well known that isothermal Taylor–Couette flow undergoes a transition to a stationary and axisymmetric toroidal vortex flow above a critical Reynolds number (Taylor 1923; Chandrasekhar 1961). Higher-order time-dependent and non-axisymmetric transitions are also observed as the Reynolds number (Re) is increased above its critical value (Andereck, Liu & Swinney 1986). These flow transitions have been the topic of numerous theoretical and computational studies. In fact, a number of investigators have been able to accurately predict these transitions (e.g. Chossat & Iooss 1985; Demay & Iooss 1984; Golubitsky & Stewart 1986; Golubitsky &

† Current address: Department of Chemical Engineering, King Fahd University of Petroleum and Minerals, Dhahran, Saudi Arabia.

Langford 1988; Demay, Iooss & Laure 1992; Jones 1982; Moser, Moin & Leonard 1983; Marcus 1984*a*, *b*; Fasel & Booz 1984; Liao, Jane & Young 1999). A summary of the most important advances in this area is provided by Tagg (1992).

The effect of energetics on the stability of Taylor–Couette flow has also been a topic of many investigations. Most prior studies have been concerned with the stability of the flow in the presence of a radial temperature gradient where an axial flow can be developed due to buoyancy. Experiments by Snyder & Karlsson (1964) have shown that for small values of the temperature difference between the inner and outer cylinders $|\Delta T|$ (i.e. $|\Delta T| < 1$ K) the flow is stabilized while for large values (i.e. $|\Delta T| > 1$ K) the flow is destabilized. Moreover, it has been observed that an imposed temperature gradient influences the structure of the secondary flow. Specifically, for small values of $|\Delta T|$ the secondary flow is similar to the isothermal flow (i.e. toroidal vortex flow) while uneven spirals are observed at large $|\Delta T|$. In addition, the neutral stability diagram has been observed to be nearly symmetric in $\pm|\Delta T|$ for small values of ΔT.

The effect of an imposed radial temperature gradient on the linear stability of the Taylor–Couette flow has also been theoretically examined by Ali & Weidman (1990) and it has been shown that for a fixed Prantdl number, Pr, the secondary flow is axisymmetric and the critical Reynolds number, Re_c, increases with increasing Grashof number Gr. However, for larger Gr values the secondary flow becomes non-axisymmetric and Re_c decreases with increasing Gr. Chen & Kuo (1990) have also performed a linear stability analysis for axisymmetric disturbances and have shown that the stability characteristics of the flow can be characterized in terms a dimensionless parameter, $C_b \equiv \beta(T_1 - T_2)(R_2 - R_1)^2\Omega/\nu$, that signifies the ratio of buoyant to viscous forces, where β is the thermal expansion coefficient, T_1 and T_2 are inner and outer cylinder temperatures respectively, R_1 and R_2 are inner and outer cylinder radii respectively, Ω is the angular velocity of inner cylinder, and ν is the kinematic viscosity of the fluid. Specifically, it has been demonstrated that increasing C_b increases Re_c for $\Delta T \equiv T_1 - T_2 > 0$ while for $\Delta T < 0$, Re_c is decreased. In addition, a non-zero C_b breaks the symmetry of Re_c versus ΔT diagram. Overall, the predictions of the linear stability analyses are in accord with the experimental observations.

The effect of energetics on the linear stability of Taylor–Couette flow when the two cylinders are maintained at equal temperatures while a constant heat source is used to drive an axial flow has also been examined (Kolyshkin & Vaillancourt 1993). It has been demonstrated that over a large range of cylinder radii ratios ($0.4 \leqslant R_1/R_2 \leqslant 0.95$) and Pr ($1 \leqslant Pr \leqslant 100$), axisymmetric disturbances are the most dangerous disturbances and the flow is destabilized as Pr and Gr are increased.

The above studies have examined the effect of energetics on transitions in Taylor–Couette flow for small- to moderate-viscosity Newtonian fluids where radial temperature gradients could lead to significant buoyant forces. Although highly viscous liquids will be less susceptible to similar transitions, energetics could still play a significant role in the stability of this class of fluids due to viscous dissipation. In fact, recent linear stability analyses for viscoelastic Taylor–Couette flow by Al-Mubaiyedh, Sureshkumar & Khomami (1999) have demonstrated that viscous dissipation gives rise to new eigensolutions with significantly lower values of onset conditions and different spatiotemporal characteristics than those predicted for isothermal viscoelastic Taylor–Couette flow. Specifically, it was shown that in the presence of viscous dissipation the primary transition is to a stationary and axisymmetric toroidal vortex flow, in contrast to the case of isothermal flow where the primary transition is to a

time-dependent and non-axisymmetric vortex flow (Avgousti & Beris 1993; Sureshkumar, Beris & Avgousti 1994; Joo & Shaqfeh 1994). Moreover, Al-Mubaiyedh *et al.* (1999) have demonstrated that the evolution of this new solution family depends on the Brinkman number Br, the Péclet number Pe, the gap width and the ratio of polymeric to total viscosity. In particular, for a fixed Br, the new solution family appears as Pe exceeds a critical value Pe^*. The value of Pe^* is lowered as Br, the gap width and the ratio of polymeric to total viscosity are increased.

The linear stability predictions of Al-Mubaiyedh *et al.* (1999) have been recently confirmed experimentally by White & Muller (2000) where a transition to a stationary and axisymmetric toroidal vortex flow was observed in a highly viscous Newtonian (glycerin) and elastic (a polyisobutylene-based Boger fluid) fluids. Moreover, in accord with the analysis, the onset conditions for the instability characterized in terms of a Deborah number, De, that signifies the ratio of elastic to viscous forces, were significantly lower than those measured for the isothermal flow.

The above studies have clearly demonstrated that thermal gradients induced by viscous heating could significantly influence the stability of Taylor–Couette flow of viscoelastic fluids. Since the thermoelastic instability observed by Al-Mubaiyedh *et al.* (1999) is due to the coupling of the radial perturbation velocity and the base-state temperature gradient, it is reasonable to expect that viscous dissipation could play a significant role on the stability of Taylor–Couette flow of highly viscous Newtonian fluids. Hence, the main objective of this study is to investigate the influence of viscous dissipation on the stability of Taylor–Couette flow of highly viscous Newtonian liquids where buoyancy-driven axial flows can be assumed negligible. Specifically, we have performed linear and nonlinear stability analysis using realistic fluid properties and geometric parameters where viscous heating effects could be significant. Moreover, through our linear stability analysis we demonstrate how the stability characteristics and onset conditions are modified in the presence of viscous heating. In turn, to ascertain the utility of linear stability analysis to predict the onset conditions observed experimentally, the nonlinear stability of the flow is also investigated using time-dependent numerical simulations.

This paper is organized as follows. In § 2, we present the governing equations and dimensionless parameters. Section 3 briefly outlines the solution procedure for the eigenvalue problem that arises from the normal-mode linear stability analysis as well as the time-dependent simulations used to examine the nonlinear stability of the flow. The results of the analyses are discussed in § 4. Finally, conclusions are presented in § 5.

2. Governing equations and dimensionless parameters

We consider the motion of a highly viscous Newtonian liquid confined between two infinitely long, concentric, and independently rotating cylinders. The cylindrical geometry is conveniently described by r, θ and z, representing the radial, azimuthal (circular) and axial directions respectively. The inner and outer cylinders, denoted by subscripts 1 and 2 respectively, have radii R_1 and R_2 and angular speeds Ω_1 and Ω_2. The gap width, $d \equiv R_2 - R_1$, and the inner cylinder velocity, $R_1\Omega_1$, are chosen as the scales for length and velocity respectively. The scales of time and pressure are given by $d/R_1\Omega_1$ and $\rho(R_1\Omega_1)^2$ respectively, where ρ is the fluid density. The temperature is made dimensionless with a reference temperature T_0, i.e. $\phi \equiv T/T_0$. In this work, all cases considered correspond to a stationary outer cylinder, i.e. $\Omega_2 = 0$.

The temperature change considered in this study is of $O(1)$ K, hence the fluid is practically incompressible and the continuity equation is given by

$$\nabla \cdot \boldsymbol{v} = 0. \tag{1}$$

The equation of motion is written in dimensionless form

$$\frac{\partial \boldsymbol{v}}{\partial t} - \boldsymbol{v} \times \boldsymbol{\omega} = -\nabla P + \frac{1}{Re}\nabla \cdot [\mathrm{e}^{\varepsilon((1/\phi)-1)}\boldsymbol{\kappa}], \tag{2}$$

where $\boldsymbol{\omega} \equiv \nabla \times \boldsymbol{v}$, $P \equiv p + \boldsymbol{v} \cdot \boldsymbol{v}/2$ and $\boldsymbol{\kappa} \equiv (\nabla \boldsymbol{v} + \nabla \boldsymbol{v}^t)$ are the dimensionless vorticity vector, dynamic pressure and rate-of-deformation tensor respectively, and p is the hydrodynamic pressure. The fluid viscosity is related to temperature by an Arrhenius relationship with ε as the dimensionless activation energy defined as

$$\varepsilon \equiv \frac{\Delta H}{R T_0}, \tag{3}$$

where ΔH and R are the dimensional activation energy and the universal gas constant respectively. The Reynolds number, Re, is defined as

$$Re \equiv \frac{\rho R_1 \Omega_1 d}{\eta}, \tag{4}$$

where η is the fluid viscosity evaluated at the reference temperature T_0. The non-isothermal effects considered in this work are due primarily to heat generation induced by viscous dissipation. The energy equation is written as follows to account for viscous dissipation:

$$PrRe\left[\frac{\partial \phi}{\partial t} + \boldsymbol{v} \cdot \nabla \phi\right] = \nabla^2 \phi + \frac{Br}{2}\mathrm{e}^{\varepsilon((1/\phi)-1)}\boldsymbol{\kappa} : \nabla \boldsymbol{v}, \tag{5}$$

where the Prantdl number, Pr, and the Brinkman number, Br, are defined as

$$Pr \equiv \frac{C_p \eta}{k} \tag{6}$$

and

$$Br \equiv \frac{\eta (R_1 \Omega_1)^2}{k T_0}, \tag{7}$$

where C_p and k are the fluid specific heat capacity at constant pressure and thermal conductivity respectively. The Brinkman number signifies the extent of viscous heating in the flow. A modification of the isothermal flow instability will take effect through the coupling between the temperature sensitivity of the fluid viscosity and the temperature gradients generated by viscous heating. Therefore, it is useful to characterize viscous heating of sensitive liquids in terms of the Nahme–Griffith number, Na. The Nahme–Griffith number signifies the ratio of temperature rise due to viscous heating to the temperature rise necessary to make a significant (i.e. $O(1)$) change in the viscosity. The Nahme–Griffith number is related to the Brinkman number in the following manner:

$$Na \equiv |\partial \eta / \partial T|_{T=T_0} (R_1 \Omega_1)^2 / k = \varepsilon Br. \tag{8}$$

For highly viscous fluids (e.g. glycerin and oils) and for characteristic shear rates, $\dot{\gamma} \equiv R_1 \Omega_1 / d$, associated with the Newtonian Taylor–Couette flow, the Péclet and Brinkman numbers are typically very large $Pe \equiv Pr\,Re \sim 10^5$ and $Br \sim 10^{-2}$ ($Na \sim 0.25$). Note that the Brinkman number is defined in (7) based on the absolute reference temperature, T_0, instead of the temperature drop ΔT. Therefore, a value of $Br \sim 10^{-2}$ (i.e. $\eta (R_1 \Omega_1)^2 / k \Delta T \sim 3$) is typically large.

Non-isothermal effects due to buoyancy have not been included in the above set of governing equations. Buoyancy-induced instabilities in Taylor–Couette flow could be of importance when the Grashof number, $Gr \equiv \rho^2 g\beta\Delta T(R_2 - R_1)^3/\eta^2$ is $O(1)$. However, in this study we are interested in examining whether a new mode of instability in the Taylor–Couette flow can be obtained in absence of buoyancy for highly thermally sensitive fluids. In fact, recent experimental studies by White & Muller (2000) have shown that for highly viscous and thermally sensitive fluids, buoyancy does not play a significant role in the onset conditions for the instability or the post-critical dynamics.

Equations (1), (2) and (5) are supplemented with no-slip boundary conditions for the velocities and constant wall temperatures at both cylinder surfaces. Moreover, for infinitely long cylinders, end effects in the axial direction could be neglected; hence, periodic boundary conditions are enforced in the axial and azimuthal directions.

The base state of Taylor–Couette flow is purely circular and the equation of motion (2) simplifies to

$$\frac{\mathrm{d}}{\mathrm{d}r}\left(\frac{1}{r}\frac{\mathrm{d}}{\mathrm{d}r}(rv_\theta)\right) - \frac{\varepsilon}{\phi^2} r \frac{\mathrm{d}}{\mathrm{d}r}\left(\frac{v_\theta}{r}\right)\frac{\mathrm{d}\phi}{\mathrm{d}r} = 0. \tag{9}$$

The steady-state and fully developed version of the energy equation (5) is a balance between conduction and viscous dissipation:

$$\frac{1}{r}\frac{\mathrm{d}}{\mathrm{d}r}\left(r\frac{\mathrm{d}\phi}{\mathrm{d}r}\right) + Br\ \mathrm{e}^{\varepsilon((1/\phi)-1)}\left[r\frac{\mathrm{d}}{\mathrm{d}r}\left(\frac{v_\theta}{r}\right)\right]^2 = 0. \tag{10}$$

Equations (9) and (10) constitute a nonlinear boundary value problem for which solutions were obtained numerically.

3. Method of solution

As mentioned earlier, we are interested in examining the linear and nonlinear stability of non-isothermal Taylor–Couette flow. The linear stability analysis is performed utilizing standard normal-mode analysis. Specifically, infinitesimally small, non-axisymmetric disturbances with axial wavenumber α and azimuthal wavenumber ξ are introduced into the steady-state solution vector $\boldsymbol{u}_{ss} \equiv (P, v_r, v_\theta, v_z, \phi)^t_{ss}$,

$$\boldsymbol{u} = \boldsymbol{u}_{ss} + \hat{\boldsymbol{u}}(r)\mathrm{e}^{\mathrm{i}(\alpha z + \xi\theta - \mathrm{i}\sigma t)}, \tag{11}$$

where $\mathrm{i} \equiv \sqrt{-1}$, σ is the eigenvalue that is, in general, complex ($\sigma \equiv \sigma_R + \mathrm{i}\sigma_I$) and $\hat{\boldsymbol{u}}(r)$ is the vector of perturbation eigenfunctions. Substitution of (11) into the governing equations and the boundary conditions described in § 2, and linearization about the steady-state solution lead to a complex generalized differential eigenvalue problem of the type

$$\boldsymbol{A}\hat{\boldsymbol{u}} = \sigma \boldsymbol{B}\hat{\boldsymbol{u}}, \tag{12}$$

where $\boldsymbol{A}$ and $\boldsymbol{B}$ are linear operators that contain the spatial information resulting from the linearization of (1), (2) and (5) along with the boundary conditions. The solution to the differential eigenvalue problem is obtained numerically using a Chebyshev pseudo-spectral collocation technique (Al-Mubaiyedh, Sureshkumar & Khomami 1999, 2000*a*, *b*). The linear stability analysis results reported in this work are based on 17 Chebyshev collocation points in the radial direction for the axisymmetric modes ($\xi = 0$). Accurate computations of non-axisymmetric modes and high Pe require a more refined discretization, i.e. 65 collocation points. All the results presented are mesh converged; the computed eigenvalues are converged up to five decimal places.

The nonlinear analysis is performed using time-dependent simulations. As will be shown in §4, over a wide range of the parameter space the most dangerous disturbances of the non-isothermal Taylor–Couette flow are axisymmetric. Hence, we have restricted our time-dependent simulations to axisymmetric flows.

The governing equations (1), (2) and (5) with boundary conditions are solved numerically using Chebyshev–Fourier spectral expansions (Canuto *et al.* 1988). Specifically, the radial direction is expanded using Chebyshev polynomials, while the axial direction is expanded using complex Fourier series, as follows:

$$u(t,r,z) = \sum_{k=-M/2}^{M/2-1} \sum_{j=0}^{N} \hat{u}_{kj}(t) \mathrm{e}^{\mathrm{i}k\alpha z} \Psi_j(r), \tag{13}$$

where Ψ_j is the Chebyshev polynomial of degree N. In this numerical procedure the unknown variables are expanded using equation (13), and a mixed Galerkin–collocation spectral method (Sureshkumar *et al.* 1994) is used to generate a system of ordinary differential equations for the spectral coefficients $\hat{u}_{kj}(t)$. Note that this system of ODEs is singular due to the incompressibility constraint. To rectify this problem, the pressure modes $\hat{P}_{00}(t)$ and $\hat{P}_{0N}(t)$ that do not affect the velocity are set equal to zero. Time integration is performed using the implicit second-order Adams–Moulton technique,

$$\frac{\mathrm{d}\hat{u}_{kj}(t)}{\mathrm{d}t} \equiv \frac{\hat{u}_{kj}(t+\Delta t) - \hat{u}_{kj}(t)}{\Delta t} = \frac{\hat{F}_{kj}(\hat{u}_{kj}(t))|_{t+\Delta t} + \hat{F}_{kj}(\hat{u}_{kj}(t))|_t}{2}, \tag{14}$$

where $\hat{F}_{kj}(\hat{u}_{kj}(t))$ are the functions obtained from the spectral expansions. Consequently, the resulting system of nonlinear algebraic equations (14) is solved for $\hat{u}_{kj}(t+\Delta t)$ iteratively using a Newton–Raphson technique. Unless specified, the time-dependent simulations results are obtained using $(N, M) = (17, 16)$, in the radial and axial directions respectively. We have used a dimensionless time step $\Delta t = 0.5$. Occasionally, we have used $(N, M) = (25, 24)$ and smaller time steps to ensure convergence. All the results presented are converged with respect to spatial and temporal discretizations.

4. Results and discussion

4.1. *Choice of fluid properties and operating conditions*

The influence of viscous dissipation on the stability of Taylor–Couette flow is considered for highly viscous Newtonian liquids. In particular, we perform our analysis using the glycerin that has been used by White & Muller (2002) to experimentally investigate the influence of viscous heating on the stability of Taylor–Couette flow. The physical properties of glycerin as functions of temperature are listed in table 1. The viscosity of glycerin is very sensitive to temperature: an increase of 1 K within the flow domain due to viscous heating will lead to a reduction of 8.7% in the viscosity. Hence, it is expected that non-isothermal effects will significantly modify the onset conditions as well as the spatiotemporal characteristics of the isothermal instability. Throughout this work, we perform all analyses using the characteristic shear rate, $\dot{\gamma} \equiv R_1\Omega_1/d$, as a bifurcation parameter since it is independent of temperature. Consequently, all dimensionless parameters are reported at T_0 for a specified $\dot{\gamma}$. We implement a moderate gap width corresponding to $\delta \equiv R_1/R_2 = 0.827$. This ratio corresponds to the geometry of the Taylor–Couette apparatus used by White

Physical property	Relationship to absolute temperature	Value at 25 °C
[1]η (Pa s)	$\eta = \eta(T_0)\exp\left(7417\left(\frac{1}{T}-\frac{1}{T_0}\right)\right)$	0.94
[2]ρ (kg m^{-3})	$\rho = -0.6089\,T + 1442.4$	1261
[2]C_P (Jkg^{-1} K^{-1})	$C_p = 6.4289\,T + 501.42$	2418
[2]k (W^{-1} m^{-1} K^{-1})	$k = 9.05\times10^{-5}\,T + 0.2584$	0.285

[1] White & Muller (2002).
[2] Incropera & DeWitt (1990).

TABLE 1. Properties of glycerin.

& Muller (2000) to experimentally investigate the influence of viscous heating on the stability of Taylor–Couette flow.

The choice of the temperature boundary conditions is also motivated by the experiments of White & Muller (2000). Specifically, the flow cell used by White & Muller (2000) has an aluminium inner cylinder and a glass outer cylinder. The temperature of each cylinder is controlled by using two independent heat baths where the temperature of each bath is maintained within ± 0.1 K of a specified temperature. It is anticipated that the temperature at the outer boundary, T_2, will be higher than the inner boundary, T_1, due to the higher thermal resistance of glass compared to aluminium. For this reason, we have considered two different Dirichlet boundary conditions for temperature, namely $\Delta T(T_2 - T_1) = 0$ and $\Delta T = 1\,^{\circ}$C.

4.2. *Linear stability analysis*

Linear stability analysis of Taylor–Couette flow in the presence of viscous heating is investigated over a wide temperature range for axisymmetric (i.e. $\xi = 0$) as well as non-axisymmetric (i.e. $\xi \neq 0$) disturbances. The analysis is performed by varying the base flow reference temperature, T_0, from 10 °C to 60 °C. The critical shear rate and the critical axial wavenumber are evaluated for each azimuthal wavenumber for different values of T_0. The critical Reynolds number is plotted as a function of the Nahme–Griffith number in figure 1. Overall, for a wide range of Nahme–Griffith numbers, the axisymmetric disturbances are the most dangerous disturbances. In the limit of small Nahme–Griffith numbers, viscous heating effects are negligible and the critical Reynolds numbers for $\xi = 0$, 1 and 2 are independent of Na and are very close to each other, reminiscent of the isothermal Taylor–Couette instability. (We have included results at small Na to demonstrate the asymptotic limit where viscous heating is negligible. However, in this limit the fluid viscosity is relatively small; hence buoyant effects might be of importance. However, the effect of buoyancy on the stability of flow is beyond the scope of the present study.) In particular, when $\Delta T = 0$ and Na approaches zero, Re_c for non-isothermal flow is increased to the isothermal critical values, $Re_c = 101.29$, 102.45 and 106.13 for $\xi = 0$, 1 and 2 respectively. Reducing the base-flow reference temperature leads to larger values of Na. Consequently, the critical Reynolds number decreases with an increase in the Nahme–Griffith number, indicating the destabilizing effect of viscous dissipation (i.e. for $Na = 0.3$, the critical Reynolds numbers for the axisymmeteric mode are

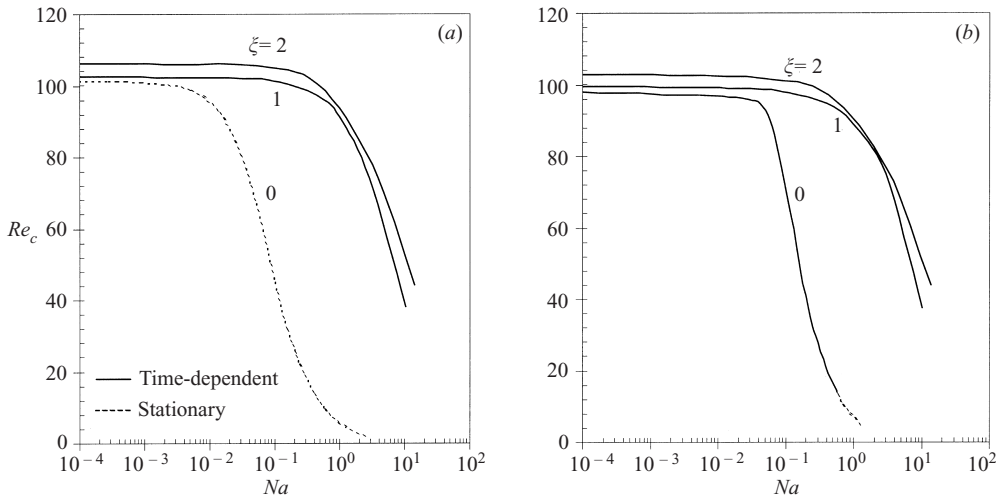

FIGURE 1. Linear stability analysis; Re_c vs. Na using the physical properties of glycerin in table 1. (*a*) $\Delta T = 0$; (*b*) $\Delta T = 1\,\mathrm{K}$.

$Re_c = 18.0$ and 28.0 for $\Delta T = 0$ and 1 K respectively). Moreover, the separation between the Re_c curves for the axisymmetric mode, $\xi = 0$, and the non-axisymmetric modes, $\xi = 1$ and 2, is significantly enhanced as Na is increased.

The temporal character of the instability is sensitive to the temperature boundary conditions. When the two cylinders are set at constant equal temperatures (see figure 1*a*), a stationary instability, that is qualitatively similar to the isothermal Taylor–Couette instability (Taylor 1923), is observed. On the other hand, when the outer cylinder is set at a higher temperature than the inner cylinder, a new axisymmetric solution family that is time-dependent is observed for $Na < 0.57$ (see figure 1*b*). For $Na > 0.57$ and $\Delta T = 1\,\mathrm{K}$, the critical eigenmode has a zero imaginary part. However, when $\Delta T > 1\,\mathrm{K}$ the critical eigenmode remains complex for all Na values investigated.

The critical axial wavenumbers, α_c, for $\xi = 0$ are plotted in figure 2 for $\Delta T = 0$ and 1 K. For $Na < 0.002$, the critical axial wavenumbers for $\Delta T = 0$ and 1 K are constant and equal to the isothermal critical value of 3.15. α_c for $\Delta T = 0$ decreases to 2.8 in the limit of large Na. Similarly, α_c for $\Delta T = 1\,\mathrm{K}$ decreases to 2.5 for $0.2 < Na < 0.57$. Consequently, the α_c curve for $\Delta T = 1\,\mathrm{K}$ undergoes a discontinuity when the stationary eigensolution family merges with the time-dependent one at $Na = 0.57$ (i.e. α_c increases to 2.8 at $Na = 0.6$). The critical frequency, σ_{Ic}, corresponding to the time-dependent instability for $\Delta T = 1\,\mathrm{K}$ is also plotted in figure 2. For small Nahme–Griffith numbers, the frequency of the secondary flow predicted by the linear stability analysis is almost constant and relatively large, $\sigma_{Ic} \sim 10^{-3}$. For $Na > 0.4$ the frequency decreases sharply to very small values (i.e. a very slow time-dependent secondary flow). White & Muller (2002) have recently performed detailed experiments to investigate the influence of Brinkman number on the stability of Taylor–Couette flow using a highly viscous mixture of glycerin and water. Their results support our observations for different values of Br. Specifically, by varying the operating temperature they observe that the vortex speed increases as the Brinkman number is reduced.

The sensitivity of the critical Reynolds number to the temperature boundary conditions is demonstrated in figure 3 for axisymmetric disturbances. Although, it is

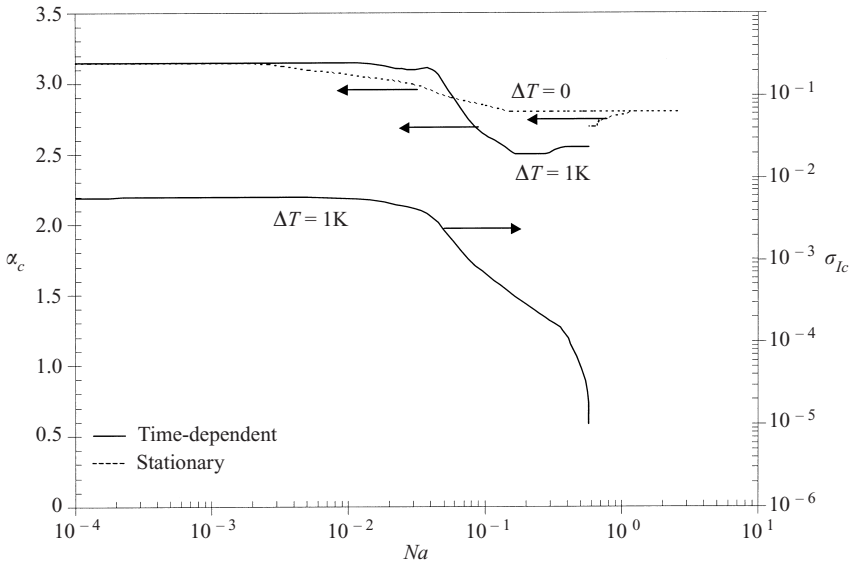

FIGURE 2. Linear stability analysis; α_c and σ_{Ic} vs. *Na* for $\xi = 0$.

expected that ΔT will be positive under the experimental conditions of White & Muller (2000), the analysis is extended here to negative values of ΔT in order to provide a complete description of the onset conditions. The temperature difference across the annular gap was restricted to relatively small values (i.e. $-1.5 \leqslant \Delta T \leqslant 1.5\,\mathrm{K}$) to minimize the effects of buoyancy. For relatively small values of $|\Delta T|$, the critical conditions correspond to a stationary mode of instability. Moreover, the neutral curve (i.e. in terms of Re_c) as a function of ΔT is not symmetric under these conditions. Specifically, as shown in figure 3(a) for $T_0 = 33\,^{\circ}\mathrm{C}$, the dependence of the critical Reynolds number on ΔT for the stationary mode is parabolic for $-1.3 \leqslant \Delta T \leqslant 0.375\,\mathrm{K}$ with a minimum at $\Delta T = -0.5\,\mathrm{K}$ for which $Re_c = 32.45$. In figure 3(b), for $T_0 = 43\,^{\circ}\mathrm{C}$ the parabolic region for the stationary mode shrinks to $-0.6 \leqslant \Delta T \leqslant 0.15\,\mathrm{K}$ with a minimum at $\Delta T = -0.375\,\mathrm{K}$ for which $Re_c = 62.63$. In addition, it is shown that for sufficiently large base-flow temperature gradients, time-dependent instabilities could be observed. As shown in figure 3, the critical Reynolds numbers for the time-dependent modes increase linearly as ΔT is increased. The frequencies of the time-dependent modes as well as the range of ΔT where they are observed increase as the reference temperature is increased. This is consistent with the earlier observation in figure 2, since the viscosity is lower at higher temperatures, leading to smaller values of the Nahme–Griffith number for which the frequency is higher.

4.3. *A comparison of linear stability predictions and experimental observations*

We performed a linear stability analysis for the non-isothermal Taylor–Couette flow at $T_0 = 18.5\,^{\circ}\mathrm{C}$ using the fluid properties of glycerin used by White & Muller (2000).† The experiment was performed using glycerin at $T_0 = 18.5\,^{\circ}\mathrm{C}$ with a viscosity of 1.36 Pa s and $Pr = 11\,000$. The transition to the secondary flow was reported at a critical Reynolds number, $Re_c = 12.75$ that is significantly smaller than the transition

† White & Muller (2002) used a glycerin sample in their experiment that contained some moisture due to long time exposure of the fluid to air. Hence we have used a slightly lower viscosity in our computations than the one indicated in table 1 (White & Muller 2000, personal communication).

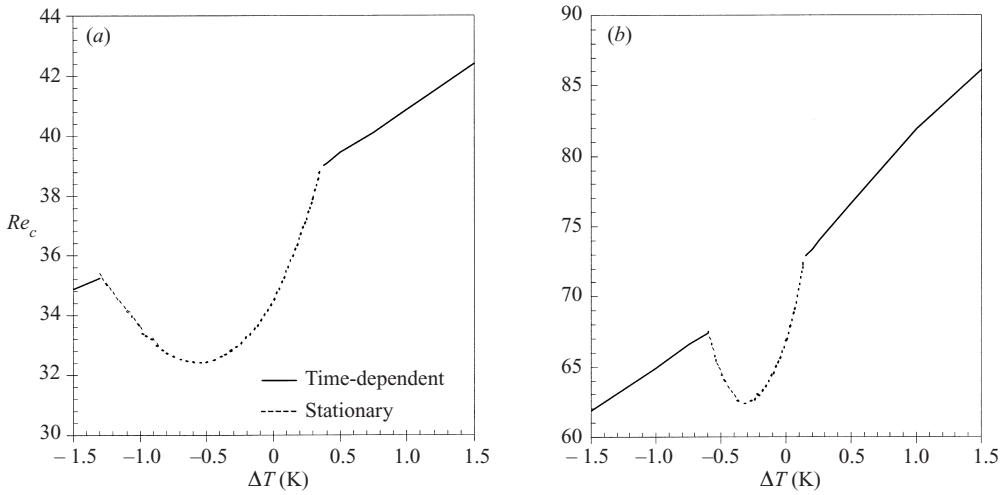

FIGURE 3. Linear stability analysis; Re_c vs. ΔT for $\xi = 0$. (*a*) $T_0 = 33\,^{\circ}\mathrm{C}$; (*b*) $T_0 = 43\,^{\circ}\mathrm{C}$.

Reynolds number observed for the isothermal Taylor–Couette flow (i.e. $Re_c = 101.29$). Moreover, the secondary flow was observed to be time-dependent and axisymmetric with vortices moving slowly parallel to the cylinder axis with a speed of approximately 0.0023 gap widths per second.

The results of our analysis clearly show that the critical Reynolds number and the spatiotemporal character of the instability depend on the base-flow temperature boundary conditions. Specifically, for $\Delta T = 0$, the critical conditions are $Re_c = 12.61$, $\alpha_c = 2.8$, $\xi = 0$ and $\sigma_{Ic} = 0$. Hence, the secondary flow is predicted to be stationary and axisymmetric. On the other hand, for $\Delta T = 1\,\mathrm{K}$, the predicted critical conditions are $Re_c = 14.32$, $\alpha_c = 2.55$, $\xi = 0$ and $\sigma_{Ic} = \pm 2.6 \times 10^{-5}$. Therefore, an axisymmetric and time-dependent secondary flow is predicted. The predicted Re_c when the two cylinders are assumed to be at an equal temperature is extremely close to the experimental value; however, the instability in this case is stationary which is in disagreement with the experimental observation. In contrast, the spatiotemporal character of the secondary flow when the outer cylinder is at a temperature 1 K higher than the inner one is similar to the experimental observation (i.e. a very slow time-dependent secondary flow). However, the predicted Re_c exceeds the experimental value by 12%. This difference can be rationalized in terms of two important factors. First, the difference could be related to experimental errors associated with measuring the onset conditions of the secondary flow (i.e. White & Muller (2000) do not report error bars associated with the measurements of the critical conditions). Secondly, it is possible that the bifurcation is subcritical. In this case, the experimentally measured critical Reynolds number can only be predicted from a nonlinear stability analysis.

Overall, our analysis clearly depicts that the onset conditions and the temporal characteristics of the classical centrifugal instability are significantly affected by viscous heating. Specifically, the transition to secondary flow in the presence of viscous heating occurs at a critical Reynolds number that is an order of magnitude smaller than the critical value for the isothermal flow. Hence, despite the minor discrepancies between the linear stability analysis predictions and the experimental observations, the dramatic destabilization of Taylor–Couette flow observed by White & Muller (2000) can clearly be attributed to viscous dissipation.

T_0	Critical parameter	$\Delta T(T_2 - T_1) = 0$	$\Delta T(T_2 - T_1) = 1\,\mathrm{K}$
33 °C	$\dot{\gamma}$	$77.63\,\mathrm{s}^{-1}$	$91.90\,\mathrm{s}^{-1}$
	α_c	2.83	2.51
	σ_{Ic}	0	2.89×10^{-4}
	Re_c	34.50	40.85
43 °C	$\dot{\gamma}$	$70.29\,\mathrm{s}^{-1}$	$86.05\,\mathrm{s}^{-1}$
	α_c	2.95	2.75
	σ_{Ic}	0	1.02×10^{-3}
	Re_c	66.91	81.90

TABLE 2. Critical states used for time-dependent simulations.

4.4. *Time-dependent simulations*

The nonlinear evolution of the non-isothermal Taylor–Couette instability is investigated by performing time-dependent simulations. In particular, a bifurcation analysis is conducted to identify the supercritical and subcritical characteristics of the secondary flow patterns. The time scale for nonlinear evolution of the non-isothermal fully developed flow is extremely large (i.e. very small temporal frequency); hence a fully implicit time integration scheme that allows large time steps has been utilized. Such an algorithm is essential in performing CPU efficient simulations.

Motivated by the difference between experimentally observed critical conditions and the linear stability predictions, we perform the time-dependent simulations using two boundary conditions for the energy equation, i.e. $\Delta T = 0$ and 1 K. The computations are performed for a fixed axial wavenumber representing the critical value obtained from the linear stability analysis. The time-periodic instabilities predicted by the linear stability analysis under the experimental conditions of White & Muller (2000) correspond to very slowly evolving secondary states. Specifically, the dimensionless frequency is very small, $\sigma_I = 2.6 \times 10^{-5}$ (i.e. an oscillation period, $t_p = 241\,661$). Since realization of a fully developed non-isothermal equilibrium state requires time integration of at least 20 periods, simulations of such slowly evolving secondary states are computationally prohibitive. Therefore, in order to gain insight into the nonlinear evolution of the non-isothermal instability, we restrict our simulations to reference temperatures where viscous effects are important and the temporal frequency of the secondary flow is larger than those corresponding to the experiments of White & Muller (i.e. $0.07 < Na < 0.2$, see figure 2). Two reference temperatures have been selected to perform the simulations, $T_0 = 33\,^{\circ}\mathrm{C}$ and $43\,^{\circ}\mathrm{C}$. The results of the linear stability analysis under these conditions are given in table 2 for both thermal boundary conditions.

The initial condition for performing the nonlinear stability analysis is constructed by superposition of the eigenfunctions associated with the most dangerous eigenvalue and the steady-state solution. In particular, for stationary instabilities we have used the following initial condition:

$$\boldsymbol{u}(t = 0, r) = \boldsymbol{u}_{ss}(r) + \mathrm{Re}(\chi \hat{\boldsymbol{u}}(r) \mathrm{e}^{\mathrm{i}\alpha z}), \tag{15}$$

where χ is chosen to ensure that the perturbation is small compared to the steady-state solution. The linear stability analysis has revealed that the leading eigenvalues for the

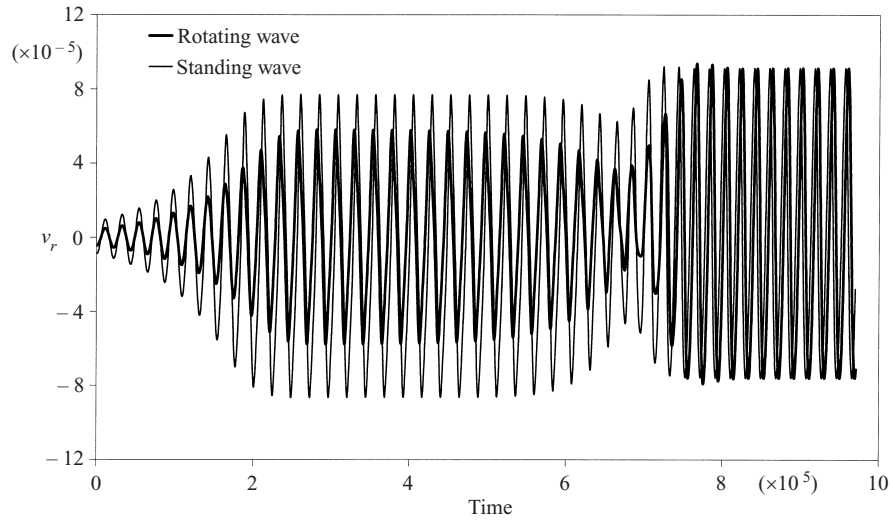

FIGURE 4. Time-dependent evolution of the radial velocity at ($r = (r_1 + r_2)/2$ and $z = \pi$) for $T_0 = 33\,^{\circ}\mathrm{C}$, $\Delta T = 1\,\mathrm{K}$, $\alpha = 2.51$ and $\dot{\gamma} = 93\,\mathrm{s}^{-1}$. Amplitude and frequency of the final states for the two different initial conditions are identical.

time-dependent instability correspond to two pairs of complex-conjugate eigenvalues. This corresponds to a degenerate Hopf bifurcation for which two possible secondary flow patterns are possible. One of the patterns corresponds to a rotating wave with axial symmetry around the z-axis, that travels axially parallel to the cylinder axis. The second pattern is that of a standing wave that oscillates horizontally in the radial direction. These flow patterns have been previously identified by considering the symmetries of the bifurcating branches after onset of instability (for more details see Golubitsky, Schaeffer & Stewart 1988, Avgousti, Liu & Beris 1993 and Sureshkumar *et al.* 1994). We have followed the same procedure as Avgousti *et al.* (1993) and Sureshkumar *et al.* (1994) in constructing the initial conditions for the time-dependent modes corresponding to either the rotating or standing wave patterns.

The simulations are performed starting from an initial condition at a shear rate that is slightly beyond the bifurcation point. Time integration is performed until an equilibrium state is reached. The time-dependent evolution of the amplitude for $T_0 = 33\,^{\circ}\mathrm{C}$, $\Delta T = 1\,\mathrm{K}$, $\alpha = 2.51$ and $\dot{\gamma} = 93\,\mathrm{s}^{-1}$ is shown in figure 4 for the rotating and the standing waves. The amplitudes corresponding to the rotating and standing waves increase gradually to different intermediate states (see the time between 200 000 and 600 000). These intermediate patterns become unstable and undergo a transition to a final time-periodic state that is independent of the initial condition. The theory of Hopf bifurcation in the presence of symmetries (Golubitsky *et al.* 1988) states that neither the rotating wave nor the standing wave solutions are stable for a subcritical Hopf bifurcation. Hence, these simulations suggest that the bifurcation is subcritical. Motivated by the temporal behaviour of the bifurcated solutions, we performed a continuation from the final state by varying the shear rate above and below the critical value. Figure 5 depicts the bifurcation diagram for the amplitude†

† In this work we define the radial velocity amplitude for time-periodic states as the difference between maximum and minimum values of the time sequence. The amplitude for stationary states is the exact value of the radial velocity. All amplitudes are evaluated at the centre of the computational domain.

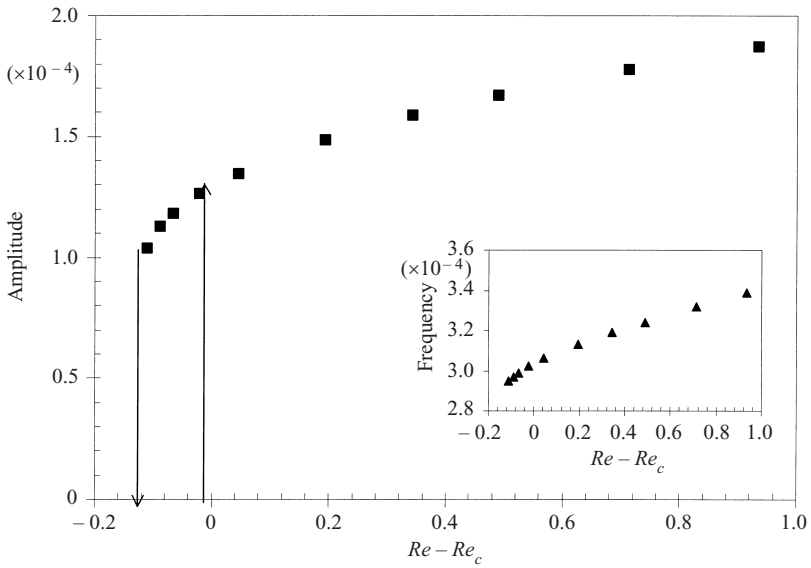

FIGURE 5. Bifurcation diagram for $T_0 = 33\,^{\circ}\mathrm{C}$, $\Delta T = 1\,\mathrm{K}$ and $\alpha = 2.51$.

as a function of $Re - Re_c$ for $T_0 = 33\,^{\circ}\mathrm{C}$, $\Delta T = 1\,\mathrm{K}$ and $\alpha = 2.51$. The bifurcation in this case is subcritical and the amplitude exhibits a hysteresis loop in the region $-0.111 < Re - Re_c < 0$. The subcritical Hopf bifurcation character of the instability is consistent with the justification provided earlier for the higher Re_c predicted by linear stability analysis for the time-dependent instability compared to the experimental Re_c value (White & Muller 2000). The frequency of the time-dependent secondary flow is also shown in figure 5. As expected, the frequency increases monotonically with shear rate. Moreover, the frequency increases linearly in the vicinity of the bifurcation point.

In figure 6, the radial velocity contours are plotted on the (r, z)-plane, for the final state in figure 4 at different times where the amplitude of the radial velocity is maximum, zero and minimum. The structure of the secondary state corresponds to axially traveling axisymmetric vortices. This structure is consistent with the secondary flow pattern that has been observed experimentally by White & Muller (2000).

The time evolution of the radial velocity at the centre of the computational domain is shown in figure 7 for the stationary instability at $T_0 = 33$, for $\Delta T = 0$, $\alpha = 2.83$ and $\dot{\gamma} = 79\,\mathrm{s}^{-1}$. This profile is similar to the isothermal case where the velocity increases to a constant value. However, the time scale to reach the final state for the non-isothermal flow is much longer than that for the isothermal flow (i.e. approximately two orders of magnitude larger). A contour plot of the radial velocity at the final state is also shown in figure 7. This structure corresponds to a stationary and axisymmetric toroidal vortex flow. The bifurcation diagram for $T_0 = 33$, $\Delta T = 0$ and $\alpha = 2.83$ is shown in figure 8. The stationary bifurcation is supercritical, similar to the isothermal flow, and the amplitude obeys the following relationship: Amplitude $= 1.9 \times 10^{-5}\sqrt{Re - Re_c}$. As the shear rate is increased, a secondary bifurcation occurs and the stationary supercritical branch undergoes a transition to a time-dependent branch at $Re - Re_c = 8.88$. The time-dependent secondary bifurcation branch has characteristics similar to the time-dependent instability for the case $\Delta T = 1\,\mathrm{K}$ (i.e. time-dependent vortices moving axially are observed; see figure 9). Overall, the frequency of the flow resulting from this secondary bifurcation is smaller than that for the case where $\Delta T = 1\,\mathrm{K}$ and it

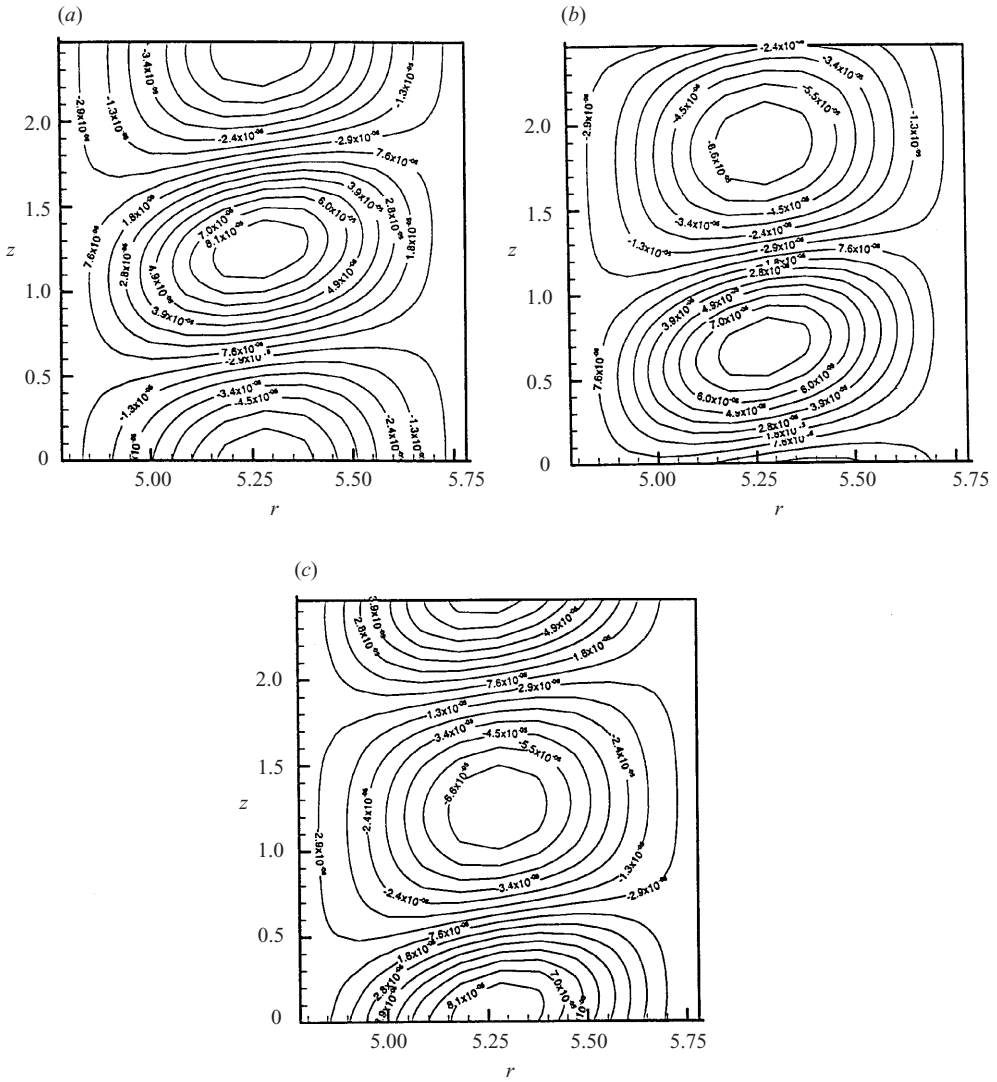

FIGURE 6. Radial velocity contours for the final state in figure 4 for $T_0 = 33\,^{\circ}\mathrm{C}$, $\Delta T = 1\,\mathrm{K}$, $\alpha = 2.51$ and $\dot{\gamma} = 93\,\mathrm{s}^{-1}$. The radial velocity v_r is shown in the (r, z)-plane in a time period where amplitude is (a) maximum, (b) zero and (c) minimum.

increases very sharply as the shear rate is increased. Moreover, there exists a hysteresis loop in the region $8.17 < Re - Re_c < 8.83$.

In order to ascertain the robustness of the predicted bifurcation structures (i.e. subcritical Hopf bifurcation for the time-dependent family and supercritical bifurcation for the stationary one), we have performed another set of simulations at a higher reference temperature, $T_0 = 43\,^{\circ}\mathrm{C}$. The bifurcation diagram and the temporal frequency of the bifurcated solution are shown in figure 10 for $T_0 = 43\,^{\circ}\mathrm{C}$, $\Delta T = 1\,\mathrm{K}$ and $\alpha = 2.75$. Similarly to the previous case, the time-dependent mode undergoes a subcritical bifurcation; however, the hysteresis loop is large ($-1 < Re - Re_c < 0$). Once again, both rotating and standing waves are unstable and they eventually evolve to the same final state. Hence, the computations at $T_0 = 43\,^{\circ}\mathrm{C}$ are consistent with

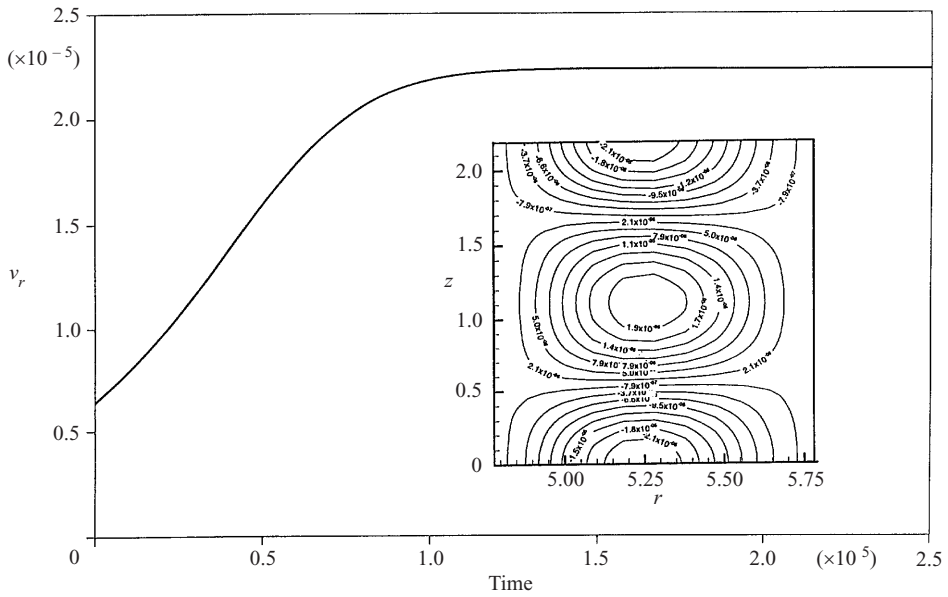

FIGURE 7. Time-dependent evolution of the radial velocity at $(r = (r_1 + r_2)/2$ and $z = \pi)$, for $T_0 = 33$, $\Delta T = 0$, $\alpha = 2.83$ and $\dot{\gamma} = 79\,\mathrm{s}^{-1}$

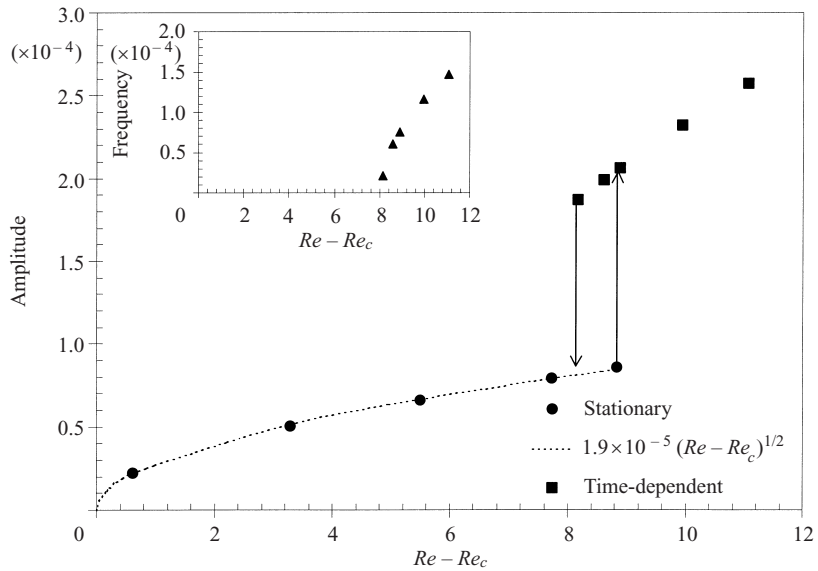

FIGURE 8. Bifurcation diagram for $T_0 = 33$, $\Delta T = 0$ and $\alpha = 2.83$.

the previous case as $T_0 = 33\,^{\circ}\mathrm{C}$. The structure of the time-dependent secondary flow at $T_0 = 43\,^{\circ}\mathrm{C}$ is qualitatively similar to the previous case with $T_0 = 33\,^{\circ}\mathrm{C}$ (i.e. axisymmetric vortices moving axially). However, the wave speed is about ten times faster in this case due to the smaller thermal diffusion time scale.

The bifurcation diagram for $T_0 = 43\,^{\circ}\mathrm{C}$, $\Delta T = 0$ and $\alpha = 2.95$ is shown in figure 11. The bifurcation of the stationary family is again supercritical and the amplitude obeys the following expression: Amplitude $= 2.65 \times 10^{-5}\sqrt{Re - Re_c}$. A

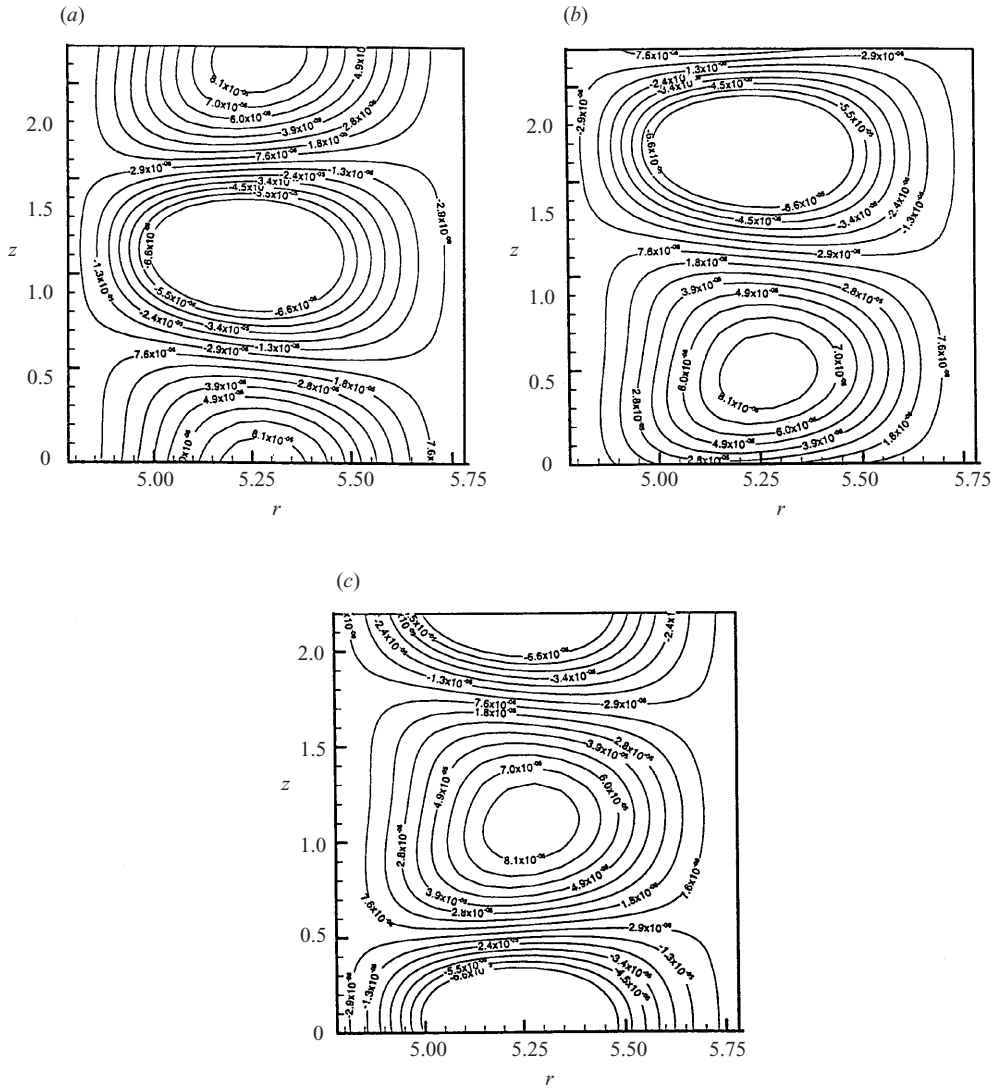

FIGURE 9. Radial velocity contours for the secondary bifurcation in figure 8 for $T_0 = 33$, $\Delta T = 0$ and $\alpha = 2.83$ and $\dot{\gamma} = 97.6\,\mathrm{s}^{-1}$. The radial velocity v_r is shown in the (r, z)-plane in a time period where amplitude is (a) maximum, (b) zero and (c) minimum.

secondary bifurcation occurs for $Re - Re_c > 10.2$ giving rise to a time-dependent flow. No hysteresis is observed for the secondary bifurcation; however, before the transition to the time-dependent state occurs, the amplitude begins to deviate from the $2.65 \times 10^{-5}\sqrt{Re - Re_c}$ curve at $Re - Re_c \approx 6.5$.

Overall, our nonlinear stability analyses at the two reference temperatures indicate similar qualitative behaviour of the non-isothermal instability. Specifically, when $\Delta T = 1\,\mathrm{K}$ the bifurcation corresponds to a subcritical Hopf bifurcation; whereas when $\Delta T = 0$ the primary bifurcation corresponds to a supercritical stationary bifurcation reminiscent of the Taylor vortex flow. Subsequently, the stationary secondary flow undergoes a bifurcation to a time-dependent flow. The flow patterns of the time-dependent states corresponding to the secondary bifurcation for $\Delta T = 0$ and the

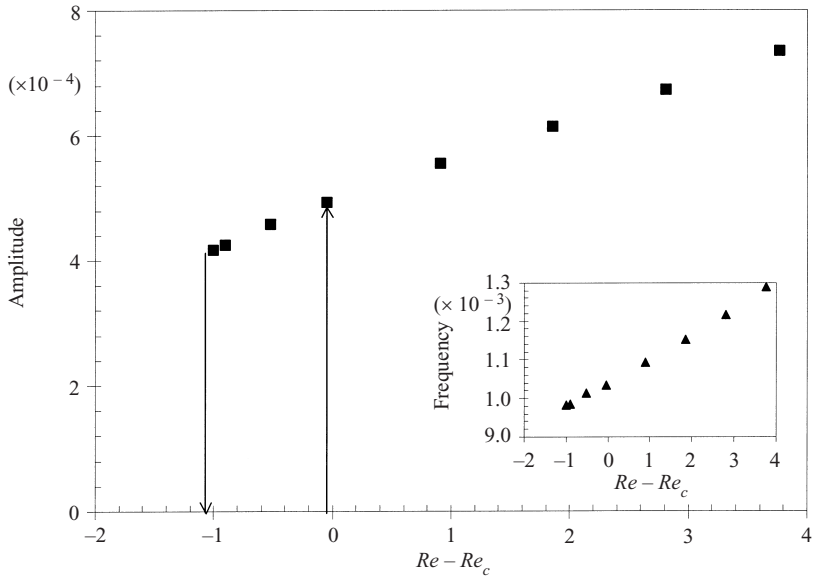

FIGURE 10. Bifurcation diagram for $T_0 = 43\,^{\circ}\mathrm{C}$, $\Delta T = 1\,\mathrm{K}$ and $\alpha = 2.75$.

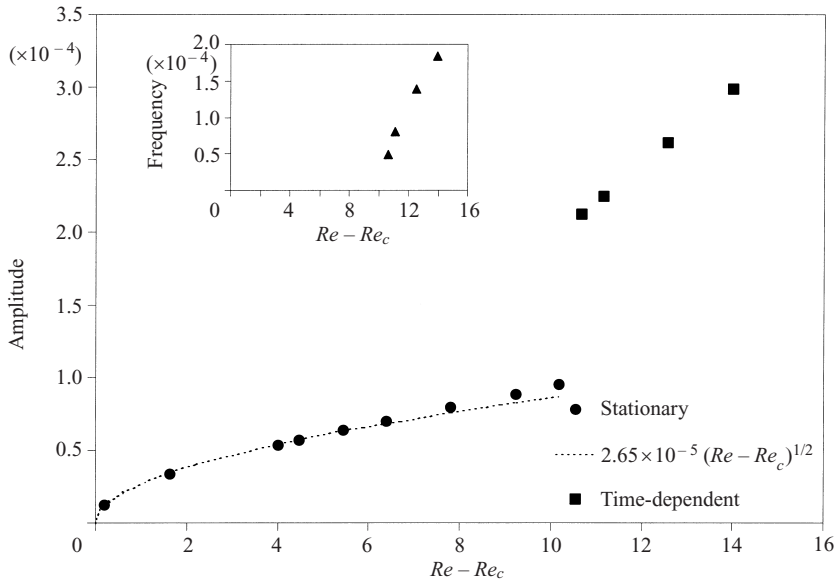

FIGURE 11. Bifurcation diagram for $T_0 = 43\,^{\circ}\mathrm{C}$, $\Delta T = 0$ and $\alpha = 2.95$.

primary bifurcation for $\Delta T = 1\,\mathrm{K}$ are similar to the experimental observations (i.e. time-dependent vortices moving axially). However, the speed of the axially moving vortices for $\Delta T = 0$ is slower. Overall, the time-dependent states observed in these simulations are similar to the experimentally observed time-dependent secondary flow (i.e. slowly moving axial vortices). However, much closer overall agreement (i.e. onset conditions and spatiotemporal characteristics of the secondary flow) with the experimental results are obtained when the thermal boundary condition $\Delta T = 1\,\mathrm{K}$ is used.

4.5. *Mechanism of the non-isothermal instability*

In this section, we discuss the mechanism of the non-isothermal instability. Our analysis is based on the linearized equations of energy and motion. In order to isolate the driving force behind the non-isothermal instability, the critical conditions are computed first, and in turn by using scaling arguments some terms are eliminated from the linearized equations and the critical conditions are re-computed. The linearized equations of energy and motion are

$$\frac{\partial \hat{\phi}}{\partial t} = -\boldsymbol{v}_{ss}\cdot\nabla\hat{\phi} - \hat{\boldsymbol{v}}\cdot\nabla\phi_{ss} + \frac{1}{Pr\,Re}\nabla^2\hat{\phi} + \overbrace{\frac{Br}{2Pr\,Re}e^{\varepsilon((1/\phi)-1)}\left(\boldsymbol{\kappa}_{ss}:\nabla\hat{\boldsymbol{v}} + \hat{\boldsymbol{\kappa}}:\nabla\boldsymbol{v}_{ss} - \frac{\varepsilon}{\phi_{ss}^2}\boldsymbol{\kappa}_{ss}:\nabla\boldsymbol{v}_{ss}\hat{\phi}\right)}^{1}, \tag{16}$$

$$\frac{\partial \hat{\boldsymbol{v}}}{\partial t} = \boldsymbol{v}_{ss}\times\hat{\boldsymbol{\omega}} + \hat{\boldsymbol{v}}\times\boldsymbol{\omega}_{ss} - \nabla\hat{P} + \frac{1}{Re}e^{\varepsilon((1/\phi)-1)}\left(\nabla^2\hat{\boldsymbol{v}} - \frac{\varepsilon}{\phi_{ss}^2}\nabla^2\boldsymbol{v}_{ss}\hat{\phi}\right) - \frac{1}{Re}\frac{\varepsilon}{\phi_{ss}^2}e^{\varepsilon((1/\phi)-1)}\left(\overbrace{\boldsymbol{\kappa}_{ss}\cdot\nabla\hat{\phi}}^{2} + \overbrace{\nabla\phi_{ss}\cdot\hat{\boldsymbol{\kappa}}}^{3} - \overbrace{(\varepsilon/\phi_{ss}^2 + 2/\phi_{ss})(\nabla\phi_{ss}\cdot\boldsymbol{\kappa}_{ss})\hat{\phi}}^{4}\right), \tag{17}$$

where the variables with a hat are perturbation quantities while the variables with the subscript *ss* are steady-state quantities. Based on a scaling argument, the influence of the viscous dissipation term (labelled 1) on the right-hand side of the linearized energy equation (16) can be ignored due to the fact that $Br \sim O(10^{-2})$ and $Pr\,Re \sim O(10^4)$. Indeed we have re-calculated the critical conditions without this term and found them to be identical to those presented in table 2 (note that the viscous dissipation terms are kept in the base flow solution). The order of magnitude of the thermal diffusion term is very small compared to the convection terms since $1/Pr\,Re \sim O(10^{-4})$. Moreover, the term $\boldsymbol{v}_{ss}\cdot\nabla\hat{\phi}$ simplifies to $v_{\theta ss}/ri\xi\hat{\phi}$, which vanishes identically since all the computed critical conditions are axisymmetric ($\xi = 0$) for the non-isothermal instability. Therefore, the remaining term, $\hat{\boldsymbol{v}}\cdot\nabla\phi_{ss}$ (i.e. coupling of the perturbation velocity with the base flow temperature gradient), on the right-hand side of the linearized energy equation appears to play a very significant role in defining the critical conditions.

Clearly, the term $\hat{\boldsymbol{v}}\cdot\nabla\phi_{ss}$ is coupled with the momentum conservation due to the thermal sensitivity of the fluid. To be more specific, a nonlinear coupling between the energy and momentum conservations arises due to the term $\nabla(e^{\varepsilon((1/\phi)-1)})\cdot\boldsymbol{\kappa}$ in (2). To demonstrate that this nonlinear coupling is the most important driving force behind the instability, we set the term $\nabla(e^{\varepsilon((1/\phi)-1)})\cdot\boldsymbol{\kappa} = 0$, and evaluate the critical conditions at $T_0 = 33\,^{\circ}\mathrm{C}$, $\Delta T = 0$ and $\delta = 0.827$. The analysis reveals that the critical conditions for $\nabla(e^{\varepsilon((1/\phi)-1)})\cdot\boldsymbol{\kappa} = 0$ are $\alpha_c = 3.15$ and $Re_c = 91.3$. These critical conditions are very different from those reported in table 2 (i.e. $\alpha_c = 2.83$ and $Re_c = 34.5$) and are very close to the isothermal case, $\alpha_c = 3.15$ and $Re_c = 101.3$. It should be noted that the critical Reynolds number reported for the case $\nabla(e^{\varepsilon((1/\phi)-1)})\cdot\boldsymbol{\kappa} = 0$ was calculated based on the viscosity evaluated at the reference temperature T_0. However, if this critical Reynolds number is rescaled by using the gap-averaged viscosity, $\bar{\eta} = \int_{r_1}^{r_2}\eta(\phi_{ss})\mathrm{d}r$, by utilizing the base flow temperature, its value is increased to 100.0. Hence, by eliminating the term $\nabla(e^{\varepsilon((1/\phi)-1)})\cdot\boldsymbol{\kappa}$, the base flow equations (9) and (10) decouple, and therefore, as expected, the onset conditions are similar to the isothermal flow.

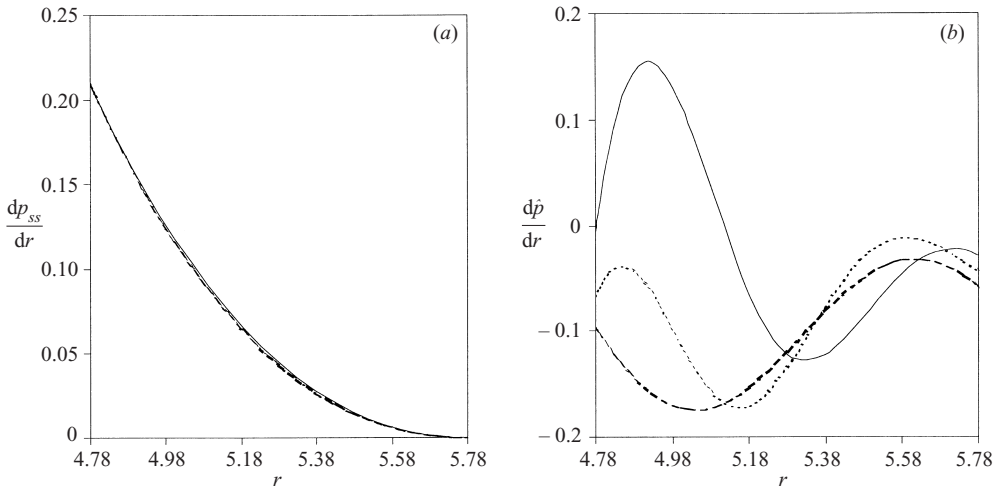

FIGURE 12. Radial pressure gradients at $T_0 = 33\,^{\circ}\mathrm{C}$ for (a) base state and (b) perturbation eigenfunctions. Isothermal, $Re = 101.3$ and $\alpha = 3.15$ (dashed curve); non-isothermal, stationary, $\Delta T = 0$, $Re = 34.5$ and $\alpha = 2.83$ (dotted curve); non-isothermal, time-dependent, $\Delta T = 1$, $Re = 40.85$ and $\alpha = 2.51$ (solid curve).

The above analysis clearly demonstrates that the term $\nabla(e^{\varepsilon((1/\phi)-1)}) \cdot \boldsymbol{\kappa}$ (terms labelled 2, 3 and 4 in the linearized equation of motion, (17)) plays a significant role in the onset conditions for the non-isothermal instability. By following an elimination procedure we have found that terms 3 and 4 are insignificant compared to term 2. Specifically, we have re-calculated the critical conditions for $T_0 = 33\,^{\circ}\mathrm{C}$, $\Delta T = 0$ and $\delta = 0.827$ after eliminating terms 3 and 4 from (17) and retaining term 2 and found them to be identical to those reported in table 2 (i.e. $\alpha_c = 2.83$ and $Re_c = 34.5$).

In the above analysis, we have clearly demonstrated that there are two important terms in the governing perturbation equations that determine the dynamics of the non-isothermal Taylor–Couette flow. The two terms are $\hat{\boldsymbol{v}} \cdot \nabla\phi_{ss}$ and $\boldsymbol{\kappa}_{ss} \cdot \nabla\hat{\phi}$. For axisymmetric disturbances, these two terms simplify to $\hat{v}_r \partial\phi_{ss}/\partial r$ and $(\partial v_{\theta ss}/\partial r - v_{\theta ss}/r)\partial\hat{\phi}/\partial r$, respectively. Hence, the mechanism of the non-isothermal instability for thermally sensitive fluids is as follows: fluctuations in the temperature are created as a result of the coupling of the radial perturbation velocity, $\hat{v}_r$, and the base-state temperature gradient, $\partial\phi_{ss}/\partial r$. In turn these temperature fluctuations significantly modify the viscosity due to the thermal sensitivity of the fluid. This in turn results in a significant reduction in dissipation of disturbances by the viscous stress terms in the momentum equation. Hence, the flow is significantly destabilized. To quantify the reduction in the dissipation provided by the viscous stress terms in the momentum equation, we have performed a mechanical energy balance on the linearized momentum equation and observed that the dissipation provided by the viscous stress terms is significantly reduced in presence of a base-flow temperature gradient.

The above mechanism suggests that the onset conditions for the isothermal Taylor–Couette instability will be modified as a result of a coupling between the momentum and the energy equations for highly thermally sensitive fluids. Since the isothermal Taylor–Couette instability is caused by the stratification of angular momentum across the annular gap, we have examined how the radial pressure gradient that is balanced by the centrifugal force is affected in the presence of significant viscous heating.

Figure 12 depicts the base-flow radial pressure gradients as well as the perturbation eigenfunctions for three cases evaluated at the critical conditions for $\delta = 0.827$.

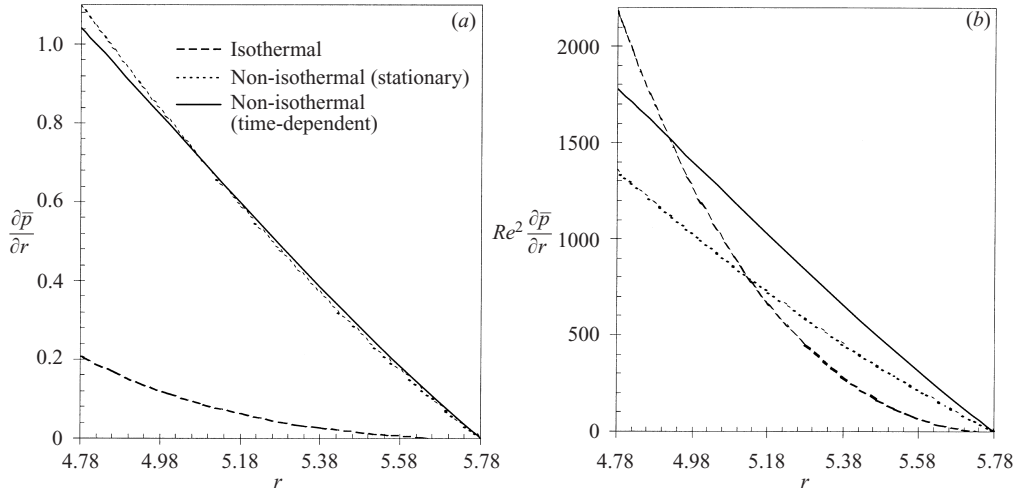

FIGURE 13. Radial pressure gradients (averaged over the axial direction) evaluated from time-dependent simulations for $T_0 = 33\,^{\circ}\mathrm{C}$. Isothermal, $Re = 102$ and $\alpha = 1.35$ (dashed curve); non-isothermal, stationary, $\Delta T = 0$, $Re = 35.11$ and $\alpha = 2.83$ (dotted curve); non-isothermal, time-dependent, $\Delta T = 1\,\mathrm{K}$, $Re = 41.34$ and $\alpha = 2.51$ (solid curve).

Clearly there is very little difference between the steady pressure gradient profiles for the three cases. This suggests that the modifications to the pressure gradient arise due to the perturbations. Specifically, one expects that in presence of thermal effects the pressure disturbances are not dissipated as effectively as the non-isothermal flow. This is illustrated in figure 12(b) where the perturbation pressure eigenfunctions for the three cases are depicted. Clearly, the fluctuations around the mean pressure are more significant for the non-isothermal cases. However, the exact enhancement of the non-isothermal pressure gradients compared to the isothermal cannot be ascertained by examining the eigenfunctions as their scale is arbitrary. Therefore, in order to ascertain the nonlinear coupling between the energetics and momentum conservation that gives rise to reduced critical Reynolds number, we have utilized the results of our time-dependent simulations. Specifically, the axially averaged (i.e. in one unit cell) radial pressure gradient that is a direct measure of the centrifugal force has been examined at shear rates slightly above the critical conditions in figure 13. Figure 13(a) shows that the dimensionless pressure drop for the isothermal flow at $Re = 102$ is significantly lower than those for the non-isothermal flows with $Re = 35.11$ for the stationary mode and $Re = 41.34$ for the time-dependent flow. Note that the pressure is made dimensionless by scaling it with $\rho(R_1\Omega_1)^2$. Therefore, the profiles were re-plotted in figure 13(b) by multiplying the average pressure gradient with Re^2 to make it independent of the inner-cylinder rotation speed. Clearly, the rescaled pressure gradients for the isothermal and non-isothermal flows are very comparable with each other. In other words, the coupling between the energetics and the momentum conservation gives rise to an enhanced centrifugal force leading to a significant reduction in the critical Reynolds number.

5. Conclusions

The influence of viscous heating on the stability of Taylor–Couette flow of highly viscous Newtonian liquids has been theoretically examined. The parameter space for the analysis has been motivated by the recent experiments of White & Muller

(2000) aimed at studying the flow transitions of a highly viscous Newtonian fluid in a Taylor–Couette device.

The stability analysis clearly depicts that viscous heating leads to significant destabilization of the flow. The instability arises as a result of viscous dissipation due to the coupling between the perturbation radial velocity with the base-state radial temperature gradient, which creates a fluctuation in the temperature gradient that couples with the momentum conservation through the base-flow shear stress giving rise to an enhanced centrifugal force and a reduction in the critical Reynolds number. The dramatic destabilization predicted by the analysis is in agreement with the experimental observations of White & Muller (2000). Moreover, if T_2 is assumed to be slightly higher than T_1 the results of the analysis are in good agreement with the experiments both in terms of the onset conditions and the spatiotemporal character of the secondary flow.

Our nonlinear stability analysis indicates that the time-dependent secondary flow (i.e. when $T_2 > T_1$) appears as a result of a subcritical Hopf bifurcation, while the stationary secondary states are the result of a supercritical bifurcation. Moreover, the qualitative structure of the predicted time-dependent secondary state agrees well with the experimental observations of White & Muller (2000), i.e. vortices moving slowly along the cylinder axis.

The significant destabilization observed in the presence of viscous hearing arises as the result of the coupling of perturbation velocities and the base-state temperature gradient that gives rise to fluctuations in the radial temperature distribution. Due to the thermal sensitivity of the fluid these fluctuations greatly modify the fluid viscosity and reduce the dissipation of disturbances provided by the viscous stress terms in the momentum equation.

U. A. M. would like to thank King Fahd University of Petroleum and Minerals at Dhahran, Saudi Arabia as well as the Arabian Oil Company for their support of his graduate scholarship. R. S. and B. K. gratefully acknowledge the Donors of The Petroleum Research Fund, administered by the ACS through grants 33297-G9 and 33203-AC9 respectively, and NSF through grants CTS-9874813 and CTS-9612499, respectively, for partial support of this research. The authors would like to thank J. M. White and S. J. Muller for providing the physical properties of glycerin.

REFERENCES

Ali, M. & Weidman, P. D. 1990 On the stability of circular Couette flow with radial heating. *J. Fluid Mech.* **220**, 53.

Al-Mubaiyedh, U. A., Sureshkumar, R. & Khomami, B. 1999 Influence of energetics on the stability of Taylor–Couette flow. *Phys. Fluids* **11**, 3217.

Al-Mubaiyedh, U. A., Sureshkumar, R. & Khomami, B. 2000*a* Linear stability of viscoelastic Taylor–Couette flow: influence of fluid rheology and energetics. *J. Rheol.* **44**, 1121.

Al-Mubaiyedh, U. A., Sureshkumar, R. & Khomami, B. 2000*b* Energetic effects on the stability of viscoelastic Dean flow. *J. Non-Newtonian Fluid Mech.* **95**, 277.

Andereck, C. D., Liu, S. S. & Swinney, H. L. 1986 Flow regimes in a circular Couette system with independently rotating cylinders. *J. Fluid Mech.* **164**, 155.

Avgousti, M. & Beris, A. N. 1993 Non-axisymmetric modes in the viscoelastic Taylor–Couette flow. *J. Non-Newtonian Fluid Mech.* **50**, 225.

Avgousti, M., Liu, B. & Beris, A. N. 1993 Spectral methods for the viscoelastic time-dependent flow equations with application to Taylor–Couette flow. *Intl J. Numer. Meth. Fluids* **17**, 49.

Baumert, B. M. & Muller, S. J. 1995 Flow visualization of the elastic Taylor–Couette instability in Boger fluids. *Rheol. Acta* **34**, 147.

Baumert, B. M. & Muller, S. J. 1997 Flow regimes in model viscoelastic fluid in a circular Couette system with independently rotating cylinders. *Phys. Fluids* **9**, 566.

Canuto, C., Hussaini, M. Y., Quarteroni, A. & Zang, T. A. 1988 *Spectral Methods in Fluid Dynamics*. Springer.

Chandrasekhar, S. 1961 *Hydrodynamic and Hydromagnatic Stability*. Clarendon.

Chen, J. C. & Kuo, J. Y. 1990 The linear stability of steady circular Couette flow with a small radial temperature gradient. *Phys. Fluids* A **2**, 1585.

Chossat, P. & Iooss, G. 1994 *The Couette–Taylor Problem*. Springer.

Demay, Y. & Iooss, G. 1984 Calcul des solutions bifurquees pour la probleme de Couette–Taylor avec les deux cylinders en rotation. *J. Mec. Theor. Appl.* (Special Issue), 193.

Demay, Y., Iooss, G. & Laure, P. 1992 Wave patterns in the small gap Couette–Taylor problem. *Eur. J. Mech.* B **11**, 621.

Fasel, H. & Booz, O. 1984 Numerical investigation of supercritical Taylor-vortex flow for a wide gap. *J. Fluid Mech.* **138**, 21.

Golubitsky, M. & Langford, W. F. 1988 Pattern formation and bistability in flow between counterrotating cylinders. *Physica* **32**, 362.

Golubitsky, M., Schaeffer, D. G. & Stewart, I. N. 1988 *Singularities and Groups in Bifurcation Theory*, vol. 2, Springer.

Golubitsky, M. & Stewart, I. N. 1986 Symmetry and stability in Taylor–Couette flow. *SIAM J. Math. Anal.* **17**, 249.

Incropera, F. P. & DeWitt, D. P. 1990 *Fundamentals of Heat and Mass Transfer*, 3rd Edn. John Wiley and Sons.

Jones, C. A. 1982 On flow between counter-rotating cylinders. *J. Fluid Mech.* **120**, 433.

Joo, Y. L. & Shaqfeh, E. S. G. 1994 Observations of purely elastic instabilities in the Taylor–Dean flow of a Boger fluid. *J. Fluid Mech.* **262**, 27.

Kolyshkin, A. A. & Vaillancourt, R. 1993 On the stability of nonisothermal circular Couette flow. *Phys. Fluids* A **5**, 3136.

Liao, C. B., Jane, S. J. & Young, D. L. 1999 Numerical simulation of three dimensional Couette–Taylor flows. *Intl J. Numer. Meth. Fluids* **29**, 827.

Marcus, P. S. 1984*a* Simulation of Taylor–Couette flow. Part 1. Numerical methods and comparison with experiments. *J. Fluid Mech.* **146**, 45.

Marcus, P. S. 1984*b* Simulation of Taylor–Couette flow. Part 2. Numerical results for wavy-vortex flow with one traveling wave. *J. Fluid Mech.* **146**, 65.

Moser, R. D., Moin, P. & Leonard, A. 1983 A spectral numerical method for the Navier–Stokes equation with applications to Taylor–Couette flow. *J. Comput Phys.* **52**, 524.

Snyder, H. A. & Karlsson, S. K. F. 1964 Experiments on the stability of Couette motion with a radial thermal gradient. *Phys. Fluids* **7**, 1696.

Sureshkumar, R., Beris, A. N. & Avgousti, M. 1994 Non-axisymmetric subcritical bifurcation in viscoelastic Taylor–Couette flow. *Proc. R. Soc. Lond.* A **447**, 135.

Tagg, R. 1992 A guide to the literature related to the Taylor–Couette problem. In *Ordered and Turbulent Patterns in Taylor–Couette Flow* (ed. C. D. Andereck & F. Hayot). Springer.

Taylor, G. I. 1923 Stability of a viscous liquid contained between two rotating cylinders. *Phil. Trans. R. Soc. Lond.* A **223**, 289.

White, J. M. & Muller, S. J. 2000 Viscous heating and the stability of Newtonian and viscoelastic Taylor–Couette flows. *Phys. Rev. Lett.* **84**, 5130.

White, J. M. & Muller, S. J. 2002 Experimental studies on the stability of Newtonian Taylor–Couette flow in the presence of viscous heating. *J. Fluid Mech.* **462**, 133.